molecular pharmaceutics

pubs.acs.org/molecularpharmaceutics

Article

Characterizing Silicone Oil-Induced Protein Aggregation with Stimulated Raman Scattering Imaging

Brian Wong, Xi Zhao,* Yongchao Su, Hanlin Ouyang, Timothy Rhodes, Wei Xu, Hanmi Xi, and Dan Fu*

Cite This: *Mol. Pharmaceutics* 2023, 20, 4268−4276

Read Online

ACCESS | Metrics & More | Article Recommendations | Supporting Information

ABSTRACT: Particles in biopharmaceutical products present high risks due to their detrimental impacts on product quality and safety. Identification and quantification of particles in drug products are important to understand particle formation mechanisms, which can help develop control strategies for particle formation during the formulation development and manufacturing process. However, existing analytical techniques such as microflow imaging and light obscuration measurement lack the sensitivity and resolution to detect particles with sizes smaller than 2 μm. More importantly, these techniques are not able to provide chemical information to determine particle composition. In this work, we overcome these challenges by applying the stimulated Raman scattering (SRS) microscopy technique to monitor the C−H Raman stretching modes of the proteinaceous particles and silicone oil droplets formed in the prefilled syringe barrel. By comparing the relative signal intensity and spectral features of each component, most particles can be classified as protein−silicone oil aggregates. We further show that morphological features are poor indicators of particle composition. Our method has the capability to quantify aggregation in protein therapeutics with chemical and spatial information in a label-free manner, potentially allowing high throughput screening or investigation of aggregation mechanisms.

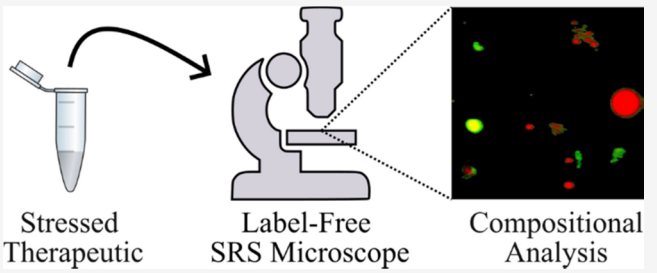

KEYWORDS: *biophysical characterization, stimulated Raman scattering, drug product particulates, protein aggregation, prefilled syringe*

INTRODUCTION

Protein therapeutics are an essential class of drugs capable of treating a variety of human diseases, such as cancer, diabetes, HIV, and autoimmune diseases.[1] They are often produced in living cells using recombinant DNA technology. The number of protein therapeutics in the clinic and development pipeline, including monoclonal antibodies, peptide hormones, cytokines, therapeutic enzymes, etc., has increased dramatically over the last decade. One challenge of developing protein therapeutics is that they have the propensity to aggregate in the formulation, which not only lowers drug efficacy but also possibly provokes an adverse immune response.[2−4] Aggregation can occur in response to chemical, environmental, or mechanical stress conditions, often caused by changes in pH, temperature, light stress, and shear force during processing or storage.[5−7] Importantly, as protein therapeutics are often formulated at high concentrations, the proteins are innately prone to aggregation. For these reasons, regulatory agencies have rigorous guidelines on the specifications of total particle counts for biological formulations. Particles in the drug products can be extrinsic (e.g., cloth fibers and plastics), intrinsic (e.g., silicone oil droplets), or inherent (e.g., protein aggregates in the formulation and particles originating from formulation composition).[8] In drug products, subvisible proteinaceous particles pose a high risk to product quality and bioavailability and have the potential to induce life-threatening immunogenicity issues.[2,9,10] Multiple pathways for aggregation exist and are dependent on numerous factors, including sample conditions, protein sequence, and protein structure.[11] Extrinsic factors such as administration method, impurities, and patient disease state have been shown to influence immune response.[3] However, which aggregate types are immunogenic is not well understood, and the causes of antidrug antibody formation remain controversial.[3,11] It has been well recognized that the chemical composition of subvisible particles may reveal the mechanism of particle formation in drug products. Unfortunately, current analytical methods used to detect subvisible particles only provide limited morphological information and often conflicting results.[12−14]

A prefilled syringe (PFS) is a well-established functional device for subcutaneous (SubQ) delivery of high-concentration biological products. Silicone oil acting as a lubricant is

Received: May 2, 2023
Revised: June 16, 2023
Accepted: June 20, 2023
Published: June 29, 2023

precoated in the PFS glass barrel to maintain its functionality. It has been reported in various studies that silicone oil is prone to migrate from the glass barrel into formulation along staging.[15−17] Importantly, previous studies have shown that silicone oil and protein molecules can interact to form protein−silicone oil particle mixtures.[18−21] Although silicone oil by itself is often considered innocuous, silicone oil−protein particle mixtures may have immunogenic properties.[22] In light of potential immunogenic concerns, efforts have been made to eliminate silicone oil in syringes to improve formulation stability through the development of silicone oil-free syringes.[23,24] Current methods to study and quantify drug solution particles include light obscuration (HIAC), microflow imaging (MFI), and imaging flow cytometry (IFC).[25−30] These industry gold standards mostly acquire morphological features such as Feret diameter, aspect ratio, circularity, and intensity.[27] IFC is capable of providing some information regarding protein−silicone particle mixing but requires fluorescent tagging, which may induce protein aggregation. All three methods lack chemical specificity in particle counting and information regarding innate particle heterogeneity.

To overcome the limitation of existing characterization techniques, we investigated whether stimulated Raman scattering (SRS) microscopy can be used to provide a detailed morphological and chemical characterization of subvisible particles from protein formulations in prefilled syringes. SRS utilizes two pulsed lasers (pump and Stokes) to generate Raman images with intensities linearly dependent on molecular concentration.[31] It has the advantage of nonperturbative imaging of heterogeneous samples with submicron spatial resolution and detailed spectral information at each pixel for compositional analysis. SRS has been widely used in biomedical imaging applications.[32−34] Applications in characterizing pharmaceutical products with SRS have also been demonstrated.[35−37] However, it has not been used to investigate protein therapeutics. Unlike biological cells or tissues, imaging protein aggregates in drug formulations is a needle-in-a-haystack problem because of the sparse nature of aggregates in the solution and thus requires a different imaging strategy.

Herein, we describe the adaptation of an SRS microscopy-based approach to study and characterize the interaction of drug protein and silicone oil in a protein therapeutic by monitoring the C−H Raman stretching modes of the active pharmaceutical ingredient (protein) and silicone oil. By comparing the relative signal intensity and spectral features of each component, the composition of most particles can be quantified and classified by least mean squares regression. We discovered that the majority of particles are protein−silicone oil mixtures. To the best of our knowledge, this is the first application of SRS microscopy to study therapeutic protein aggregates. Our developed method has the capability to quantify aggregation in protein therapeutics with chemical and spatial information in a label-free manner. The described technique can be adapted for particle screening and to study aggregation mechanisms.

MATERIALS AND METHODS

SRS Microscope System. The details of the SRS microscope have been previously described.[38,39] Briefly, the system (FLINT FL2, Light Conversion) outputs a 1030 nm beam with a 77 MHz (f0) repetition rate. This beam is split by a polarizing beam splitter into two arms: one arm is sent to an optical parametric oscillator (OPO) to generate the wavelength tunable pump beam (790 nm), and the other acts as a Stokes beam (1030 nm). The Stokes beam is modulated at 19.25 MHz (f0/4) by an electro-optical modulator (EOM). The Stokes beam is chirped by a grating-based pulse stretcher. The pump beam is dispersed using 60 cm of dense flint glass rods (SF11, Newlight Photonics). The two beams are combined with a dichroic mirror and then sent to a homebuilt upright laser scanning microscope. A schematic of this microscope setup is shown in Figure 1A. Images are taken

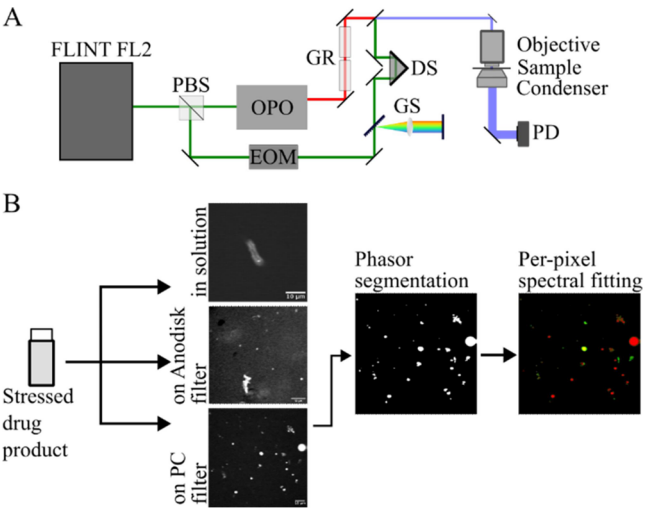

Figure 1. (A) Schematic drawing of the hyperspectral SRS (hsSRS) setup based on a femtosecond laser system. Abbreviations: DS, delay stage; EOM, electro-optical modulator; GR, glass rod; GS, grating stretcher; OPO, optical parametric oscillator; PBS, polarizing beam splitter; PD, photodiode. (B) Schematic of the sample imaging workflow. Stressed protein therapeutic is imaged in three approaches: in solution, on an Anodisk filter, and on a PC (polycarbonate) filter. Following imaging on the PC filter, a phasor is used to segment particles, and the image after segmentation is fed through a nonnegative least-squares regression fitting to extract particle composition at a per-pixel level.

with either a 25×, 1.05 NA objective (Olympus, XLPLN25XWMP2) or a 40×, 1.15 NA objective (Nikon, N40XLWD-NIR). Powers are set to 20 mW pump (790 nm) and 40 mW Stokes (1030 nm) at the focus for imaging with the Anodisk filter. Images taken with the polycarbonate (PC) filter have powers at 20 mW pump and 20 mW Stokes. All images are collected at room temperature.

Sample Preparation. Etanercept (Enbrel) 50 mg solution for injection in prefilled syringes was placed on a shaker agitating at 300 rpm under room light and at room temperature for 14 days to facilitate aggregate formation. The etanercept solution was then pulled from PFS syringes and stored at −80°C. Samples were thawed to room temperature before characterization.

MFI Imaging. Subvisible particulate data were collected using MFI 5200 (Protein Simple; Santa Clara, CA, USA). For each sample, a sample volume of 0.9 mL was used for each of the three runs, and the result was reported as an average of the three runs. The number of particles per mL was measured in the size ranges of ≥2, 2−5, ≥5, 5−10, ≥10, and ≥25 μm. The silicone oil particles were sorted by applying a filter with an aspect ratio of ≥0.85.

https://doi.org/10.1021/acs.molpharmaceut.3c00391
Mol. Pharmaceutics 2023, 20, 4268−4276

Sample SRS Imaging Preparation. Particles present in drug solution were first imaged in free solution. Slides were prepared by sandwiching a microscope glass coverslip and glass cover slide between two strips of double-sided tape to form an empty channel. 30 μL of drug solution was then pipetted into the channel, followed by sealing the edges of the sample with nail polish. The sample was then transferred to the SRS microscope for imaging.

For filter immobilized particle imaging, 0.2 μm pore size, 25 mm Whatman Anodisk inorganic filter membranes (WHA68096022) and 0.2 μm pore size, 25 mm PC membrane filters (GTTP02500) were purchased from Sigma Aldrich. Both filter materials followed the same sample preparation. 300 μL of drug solution was vacuum filtered through the filter. The filtering step acts to both immobilize and enrich the number of particles for optical assessment. Following vacuum filtration, the filter is carefully removed and placed onto a glass slide. Three drops of additional drug solution were added to the filter for optical transparency. Next, a coverslip was placed on top of the filter to sandwich it. The filter was then sealed with nail polish to prevent movement and dehydration. The sample preparation and imaging workflow are shown in Figure 1B.

Phasor Analysis for Particle Segmentation. The phasor approach to analyze hyperspectral SRS images was accomplished as described by Fu and Xie.[40] The 3D SRS hyperspectral image stack can be projected onto a 2D phasor plot by computing a Fourier transform for each pixel. The real and imaginary components of the resulting first harmonic of the Fourier transform are used as positions in a scatter plot in phasor space. In this manner, each point on the phasor plot corresponds to a specific spectrum, and spectral similarity will manifest as spatial closeness in the phasor plot. The phasor approach was used to segment out regions of interest for particle identification. The phasor region corresponding to aggregate particles was empirically chosen to segment out most particles while removing obvious contaminants based on particle spectral analysis. Pixels from the imagebackground were represented by the high-intensity region in the phasor plot and the far ends of the phasor represent different chemical species. Therefore, phasor selections that encompassed the bottom and near the background phasor showed the best performance in separating particles from the background (Figure 3A). Mixtures of silicone oil and protein particles exist in the space between the most distant cluster of silicone oil spectra and the background high-intensity centroid region. We utilized a rectangular shape for phasor ROI selection for the ease of testing different phasor regions for best particle segmentation. Different ROI shapes may be used depending on how similar the spectra are for segmentation. Appropriate phasor segmentation masks will only contain silicone oil droplets, protein particles, and mixtures of these two particles. Once the segmentation mask was generated, the Analyze Particles tool in ImageJ was used to choose regions of interest.

Compositional Analysis. The particle compositions were determined using nonnegative least mean squares regression fitting. Each particle was assumed to be a combination or solely composed of silicone oil and protein. The composition of the particle can then be represented by fitting the spectra of each pure component to the particle spectrum. The curve fitting was performed using the lsqnonneg function in MATLAB. For the PC filter images, the contributions from the filter were removed by subtracting the PC Raman spectrum after scaling by the isolated peak at 3065 cm^{-1}. The fitting takes in inputs of the basis compositional Raman spectra which in this case was pure silicone oil and pure protein solution. The output is a fitting of the input basis spectra to the sample spectra.

Pearson Correlation Coefficient (PCC) Analysis. Following phasor segmentation to generate ROIs in ImageJ, we utilized the Analyze Particles tool in ImageJ to extract morphological metrics of area, circularity, Feret diameter, aspect ratio, roundness, and solidity of each particle. Using these size metrics and the silicone oil percentages of each particle determined by fitting, we used the corrcoef function in MATLAB to generate a matrix of correlation coefficients with values ranging from −1 to +1 for both filter imaging sessions. Values closer to −1 indicate a negative linear correlation, 0 indicates no linear correlation, and +1 indicates a positive linear correlation.

RESULTS AND DISCUSSION

MFI and IFC have previously been successfully applied to monitor aggregation in protein therapeutics.[25−27] However, these methods rely on fluorescent tagging or solely morphological features to classify particle identity. Unlike these methods, SRS allows for direct chemical imaging, spectrum-based identification, and subvisible particle imaging at submicron spatial resolution. Through combining SRS imaging and particle filtration, we are able to reliably image intraparticle heterogeneity and the silicone oil−protein interaction of subvisible particles >2 μm.

Stressed drug solutions were first imaged with MFI to count the number of particles in the solution. In 1 mL of solution, MFI reports that 13,511 (40%) particles were protein, and 20,227 (60%) particles were silicone oil between 2 and 10 μm in size. Smaller particles are difficult to capture and classify with MFI. The classification is based on morphological features. Following MFI, the drug solution was directly imaged by SRS. In SRS imaging, floating particles in the solution showed significant heterogeneity in both morphology and chemical composition. The particles imaged can be classified into three general categories: silicone oil−protein mixture, silicone oil, and proteinaceous. Interestingly, for silicone oil−protein mixture particles, intraparticle heterogeneity is apparent. Many particles have clear regions of silicone oil droplets present within, whereas others have more interspersed silicone oil Raman signatures. Representative of this class of particles, Figure 2A has bright silicone oil spots on the left of an aggregated particle, with the bulk of the particle having a lower silicone oil signature. Generally, silicone oil particles are homogeneous and have high circularity with two Raman peaks at 2900 and 2960 cm^{-1} (Figure S1). In contrast, proteinaceous particles are irregularly shaped and only have one Raman peak at 2930 cm^{-1}. Figure 2B shows the SRS spectra of these particles' principal components (silicone oil in purple, protein in yellow, and silicone oil−protein mixture in green).

Initially, particles floating in the solution were found and imaged by scanning the microscope focus through the solution. Directly imaging solution is difficult because proteinaceous particles have low contrast due to background interference from the protein solution. The second challenge is keeping particles stationary for hyperspectral SRS imaging as particles would move out of optical focus due to Brownian motion. To address the first problem, we located particles in a solution with high throughput using darkfield microscopy and recorded particle locations on the sample slide. These registered particle locations were then sampled by the SRS microscope for

https://doi.org/10.1021/acs.molpharmaceut.3c00391
Mol. Pharmaceutics 2023, 20, 4268−4276

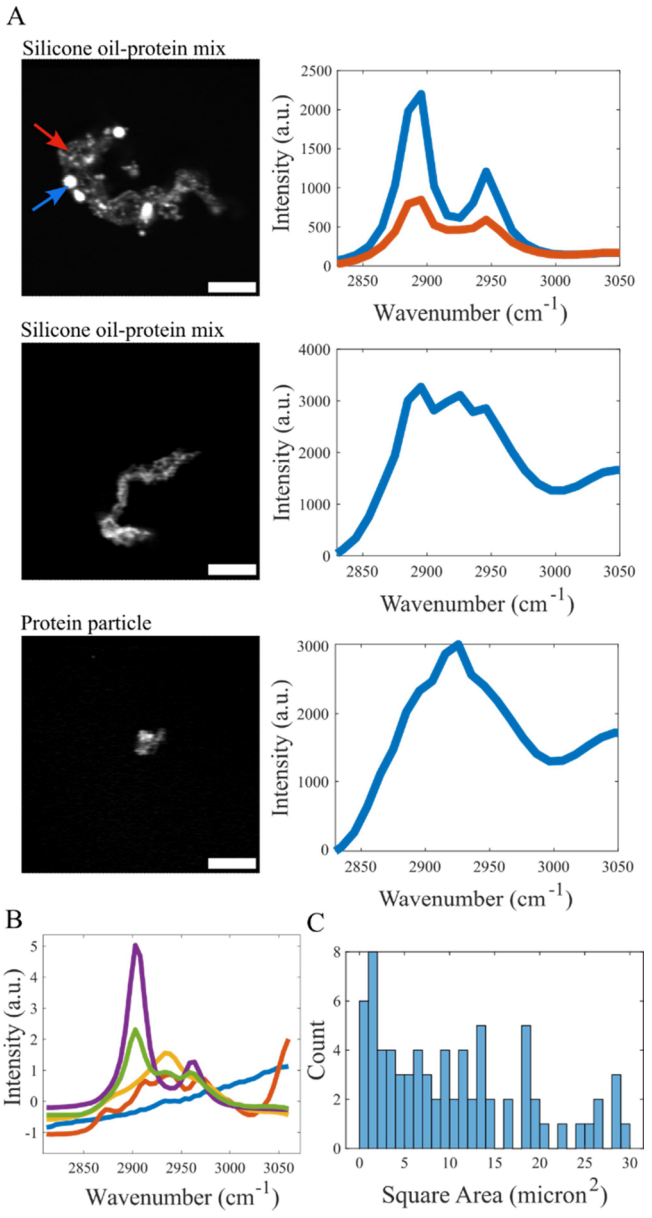

Figure 2. (A) SRS images of proteinaceous particles with varying levels of silicone oil content at 2900 cm^{-1} and accompanying spectra. Scale bars 10 μm. (B) Expected SRS spectra of the principal components of particles found. Purple, silicone oil; yellow, protein; green, silicone oil−protein mixture; blue, Anodisk filter; red, PC (polycarbonate) filter. (C) Size histogram of the 132 particles found in the solution.

imaging. Even with this increase in throughput by darkfield microscopy, the process of direct solution imaging is challenging due to low particle contrast and high particle movement. A total of 132 particles were directly imaged from ~20 μL solution and their sizes were measured (Figure 2C). These particles varied drastically in size ranging from <1 to 30 μm and shape from spherical to rod-like. Aspherical particles like those shown in Figure 2A tend to either be a mixture of silicone oil−protein or solely proteinaceous in spectral composition. From top to bottom in Figure 2A, the particles have a circularity of 0.223, 0.234, and 0.76. Interestingly, these morphological features have no appreciable relationship to the spectral character of these particles, with the top particle having large amounts of silicone oil mixing, the middle particle having little silicone oil mixing, and the bottom particle having no silicone mixing based upon the spectral shape only. This nonuniformity of composition indicates that classifications based solely on morphology are inaccurate and miss information on silicone oil components. In addition, as shown in Figure 2C, many particles were below 2 μm and thus were not detected in conventional MFI.

Filtration methods to quantify particulate matter have been previously demonstrated to identify small microplastics with Raman imaging.[41,42] Filtration improves the imaging efficiency by allowing particles to stick upon the filter surface which provides: (1) increased imaging reliability as particles are less prone to motion artifacts, (2) increased imaging throughput as particles are enriched on the filter and more likely to be in the same depth of focus. After imaging immobilized protein aggregates on the filter, we used a phasor approach to segment particles in the image and quantify their distribution. A phasor utilizes a Fourier transform to plot the spectra of each pixel as a point in the phasor plot space. Pixels of a similar spectra group are together and dissimilar spectra are further apart. As shown in Figure 3A, the high-intensity centroid is the background

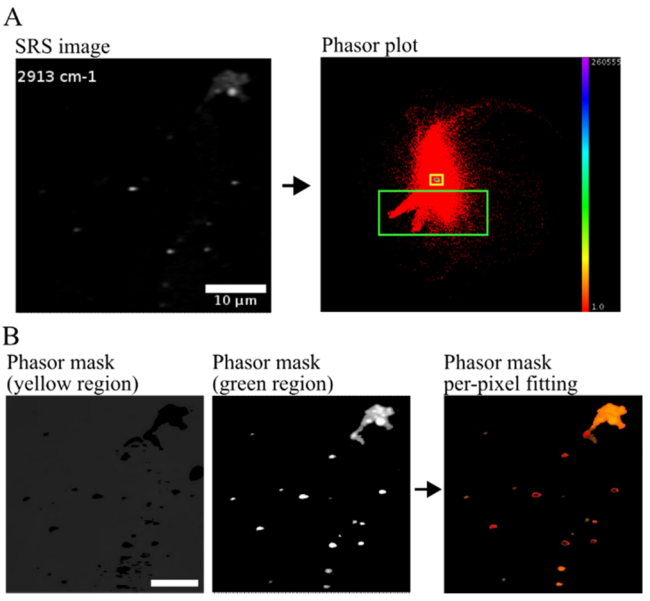

Figure 3. Visualization of the workflow from hyperspectral SRS image to phasor for segmentation. Scale bars 10 μm. (A) Phasor plot generated from the raw hsSRS image using the ImageJ spectral phasor plug-in. (B) Resultant phasor segmentation from the yellow and green bounding box. The segmentation mask from the green phasor is used to generate a per-pixel fitted image.

spectra of the filter, and the areas surrounding this region correspond to particle spectra. After segmentation, particles were analyzed at a per-pixel level to reveal particle compositional heterogeneity (Figure 3B). To test if the filter interferes with SRS measurements, the background SRS spectrum was recorded for the Anodisk filter in distilled water. As shown in Figure 2B, the SRS spectrum of the Anodisk filter (blue) is flat with no Raman peaks in the C−H region and thus does not interfere with particle spectral analysis. Following the phasor segmentation of particles, a per-pixel nonnegative linear least-squares fitting was performed with silicone oil and protein

https://doi.org/10.1021/acs.molpharmaceut.3c00391
Mol. Pharmaceutics 2023, 20, 4268−4276

solution as the basis spectral components to quantify particle compositional heterogeneity.

An Anodisk filter was first used to image 50 fields of view (Figure 4A). A total of 7042 particles were segmented for compositional analysis. These particles averaged a size of 2.85 μm (Figure 4B). Interestingly, a majority of particles (>50%) showed a mixture of silicone oil and protein with an average composition of 10−30% silicone oil. In contrast, for particles between 2 and 10 μm, MFI distinguished 40% of particles to be protein and 60% to be silicone oil, and the compositional mixing cannot be determined by MFI alone. Overall, over 90% of particles showed >10% silicone oil composition with SRS imaging. These results (Figure 4C) indicate that silicone oil plays a critical role in forming proteinaceous particles in the drug solution. Interestingly, most particles not only are a mixture of both silicone oil and protein but also exhibit significant heterogeneity in composition within the particle. Many particles showed significant amounts of silicone oil−protein mixing with several silicone oil droplets surrounded by protein clumps, similar to what is observed in the solution, suggesting that binary classification into protein and silicone oil is not sufficient in characterizing particle features. We also note that while filtration with the Anodisk filter massively increased imaging throughput, the filtration step also introduced many absorptive contaminating particles. These contaminant particles are small (Figure S2A) and have high signals but lack spectral features resembling known components (Figure S2B). Spectral phasor analysis can remove most of these contaminants. Additionally, segmentation with a spectral phasor removes any particles (such as glass flakes) that do not have a spectrum similar to silicone oil or protein spectra. However, even with a spectral phasor to segment particles, the large quantity of these absorptive contaminants vastly complicates automated analysis. These contaminants are suspected to originate from the filter. It should also be noted that images are in 2D and may not represent the entire 3D structure of the particles.

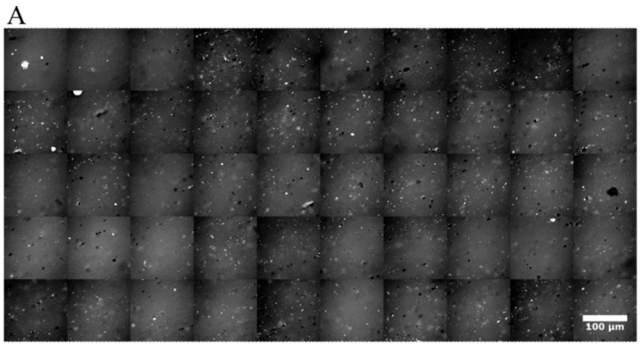

C

Percent Silicone Oil Composition	Particle Count	Percentage of Total Particles
0-10%	659	9.36
10-20%	2859	40.6
20-30%	1255	17.82
30-40%	529	7.51
40-50%	681	9.67
50-60%	384	5.45
60-70%	205	2.91
70-80%	149	2.12
80-90%	91	1.29
90-100%	230	3.27
Total Count	7056	

Figure 4. Anodisk filtration imaging dataset. (A) Mosaic tiled SRS images of particles on an Anodisk filter. Scale bar 100 μm. (B) Size histogram of the 7056 particles found with Anodisk filtration. (C) Table demonstrating percent composition of particles.

Alternative filters were tested to mitigate the absorptive contaminant problem of the Anodisk filter. Among the filters tested, the PC filter was determined to provide minimal contamination. However, in contrast to the Anodisk filter, the PC filter has strong peaks around the protein Raman peak (2930 cm^{-1}), as shown in Figure 2B. To remove the PC filter contribution to the particle spectra, the PC spectrum was removed from each pixel by subtracting the PC spectrum normalized to the isolated peak at 3065 cm^{-1}. Fifty images were taken on the PC filter (Figure 5A). As shown in Figure 5B, silicone oil droplets surrounded by proteinaceous strands can be visualized. A total of 911 particles were segmented out using the same phasor analysis as the Anodisk analysis. These particles averaged 9.92 μm in size (Figure 5C). Compared with the Anodisk filter, the particles imaged on the PC filter are

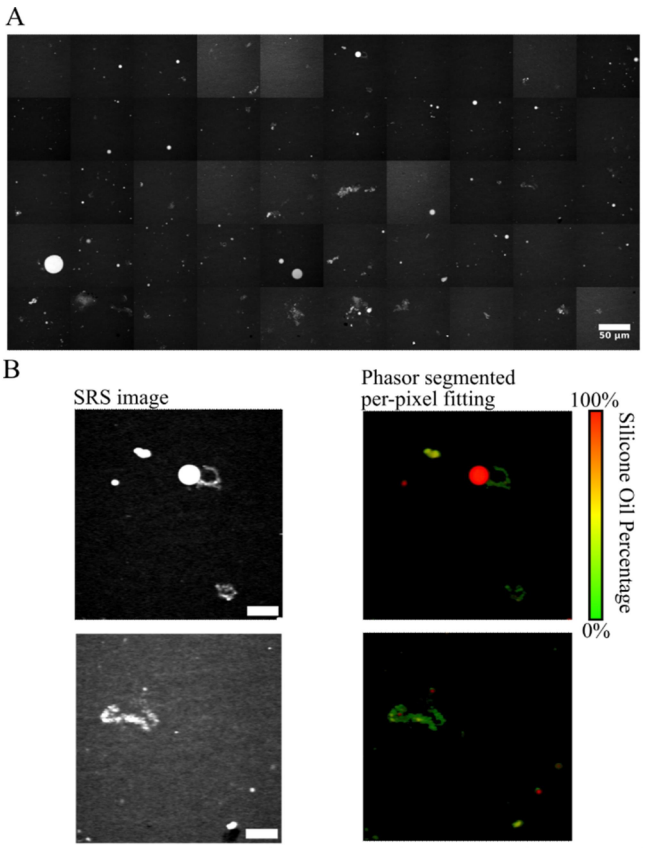

Percent Silicone Oil Composition	Particle Count	Percentage of Total Particles
0-10%	89	9.77
10-20%	146	16.03
20-30%	84	9.22
30-40%	95	10.43
40-50%	146	16.03
50-60%	122	13.39
60-70%	91	9.99
70-80%	51	5.6
80-90%	43	4.72
90-100%	44	4.83
Total Count	911	

Figure 5. Polycarbonate (PC) filter imaging dataset. (A) Mosaic tiled SRS images of particles on a PC filter. Scale bar 50 μm. (B) SRS images and accompanying pixel fitting after phasor segmentation. Red indicates silicone oil content; green indicates protein content. Scale bar 15 μm. (C) Size histogram of the 911 particles found with PC filtration. (D) Table demonstrating percent composition of particles.

https://doi.org/10.1021/acs.molpharmaceut.3c00391
Mol. Pharmaceutics 2023, 20, 4268−4276

significantly larger. This may be because many smaller particles are filtered out in the phasor segmentation due to the strong PC background. This may also be due to that the PC filter does not retain small particles as well as the Anodisk filter or that the Anodisk filter induces further aggregation. Nevertheless, consistent with previous imaging conditions, PC-filtered particles also showed significant silicone oil−protein mixing (Figure 5D). Over 90% of the particles imaged showed >10% silicone oil composition. PC filtration imaging demonstrated no absorptive particle contamination but did show contamination from the environment. A few fields of view had large lipid clumps from cover glass contamination by handling. These contaminants were easily removed manually as they have large size (several hundred μm^2 in area) and strong lipid Raman signatures at 2850 cm^{-1}. Importantly, for both tested filter materials, intraparticle chemical heterogeneity is directly visualizable with direct SRS imaging at a submicron scale (Figures S3 and S4).

To quantify the relationship between morphological metrics and spectral composition of particles, PCC tables were used to compare the shape metrics commonly used in MFI classifications such as area, circularity, Feret diameter, aspect ratio, roundness, and solidity with the spectrally fitted silicone oil composition. As shown in Tables 1 and 2, there is a lack of correlation between morphology and particle composition: no shape metric demonstrated a correlation greater than 0.3 with composition. These results provide further evidence that morphological classifications can be misleading for understanding the chemical nature of particles. Most classifications of MFI data rely only on morphological features.[29,30] Although MFI captures the overall size and shape of particles at high throughput, it has difficulty distinguishing intraparticle features due to poor imaging resolution.

As seen in Figure 6A, protein particles are distinguishable from silicone oil due to their low circularity, but any silicone oil mixing is easily missed. In contrast, SRS microscopy readily captures intraparticle heterogeneity at both the morphological and compositional levels. For example, in Figure 6B, a similarly shaped protein particle shows significant mixing with silicone oil droplets inside of the particle. It should be noted that the green region surrounding the silicone oil could either be protein on the silicone oil surface or an artifact of SRS imaging. SRS imaging has a limited spatial resolution. Such a limitation gives rise to artifacts near the edge of particles. For example, at the immediate surface of silicone oil, the sampling voxel will see a mixture of silicone oil and protein in the solution and, thus, report the presence of the protein surrounding silicone oil. This problem is further compounded by other non-Raman contributions such as cross-phase modulation near surfaces with larger refractive index discontinuity, which additionally contributes to erroneous signals. Therefore, careful consideration must be taken to observe the silicone oil−protein interactions at interfaces.

Previously, Probst has reported silicone oil−protein complex formation with IFC.[19] In their work, fluorescence labeling was used to discriminate silicone oil and protein particles in

Table 1. PCC Table for the Anodisk Filter from the Shape and Spectrally Fit Metrics from the 7056 Particles Found with Anodisk Filtration

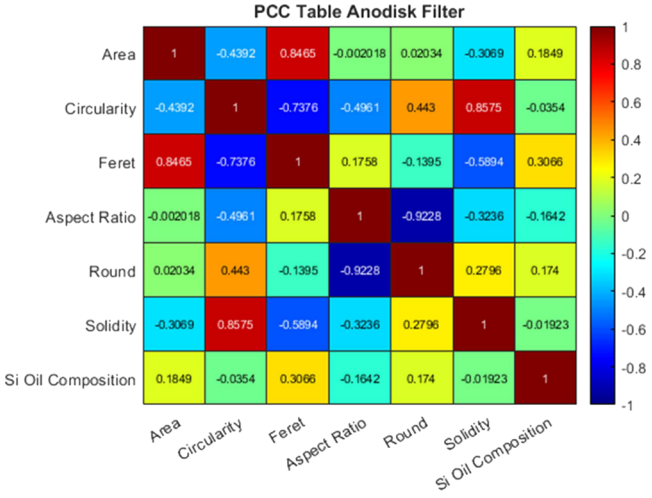

Table 2. PCC Table for the PC Filter from the Shape and Spectrally Fit Metrics from the 911 Particles Found with PC Filtration

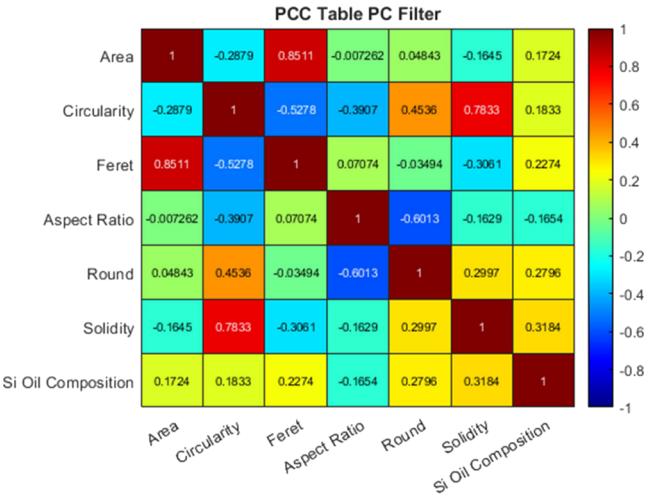

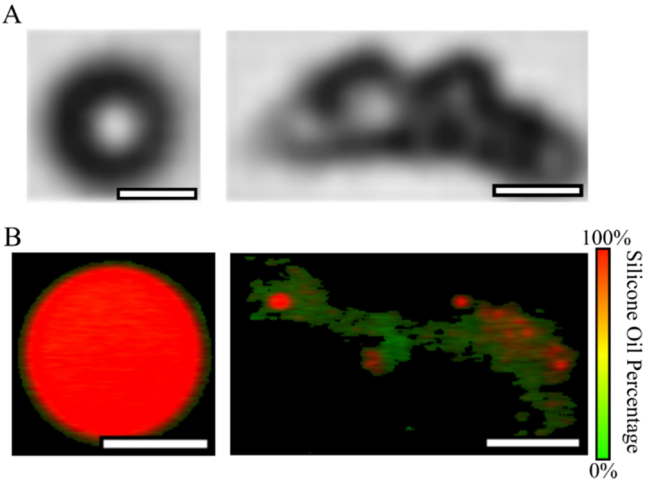

Figure 6. Comparison of similarly shaped particulate in the drug solution. Scale bar 10 μm. (A) MFI images of a single silicone oil (left) and a single protein (right) particle. (B) SRS image after phasor segmentation and fitting of a single silicone oil (left) and a silicone oil−protein (right) particle. Color represents the percentage of silicone oil components at a pixel level with green representing the protein component and red representing the silicone oil component of the particle.

https://doi.org/10.1021/acs.molpharmaceut.3c00391
Mol. Pharmaceutics 2023, 20, 4268−4276

formulation. Silicone oil−protein mixture formation and protein coating of silicone oil droplets were observed, but detailed mixing and chemical information was not available. Krayukhina et al. reported a loss of soluble protein with etanercept reconstituted in silicone oil containing water for injection.[43] They also indirectly showed evidence for etanercept being adsorbed on the surface of silicone oil with evidence suggesting that this adsorption activates immune cells. In corroboration with these previous studies, we have visualized the mixing interaction that occurs between etanercept and silicone oil droplets to form silicone oil−protein aggregates by directly imaging the silicone oil−protein interactions in a near-native particle environment without the addition of extrinsic dyes or tags. The additional capability of SRS to examine intraparticle composition at the submicron resolution will allow for more comprehensive studies of silicone oil−protein interactions.

CONCLUSIONS

Understanding how protein therapeutics form potentially immunogenic particles is important to improve product development and enhance quality control for these important drugs. A major challenge in analyzing protein aggregates lies in the unknown nature of the formed aggregates as well as the wide size range. Current methods (e.g., MFI) classify and screen particles based on their morphological and size metrics. Such metrics can be ambiguous in the case of silicone oil−protein particle mixtures. Here, we developed a new workflow utilizing SRS microscopy to study the composition of subvisible particles in protein therapeutics. Particles in the stressed protein solution in a prefilled syringe are from two basic components: silicone oil and protein. By fitting the C−H SRS spectra of these components to the imaged particles, we determined the composition of each particle. This approach enables the identification of drug product aggregates unambiguously with chemical and spatial information in a label-free manner. Moreover, spatially resolved chemical composition analysis provides additional information about the intraparticle compositional heterogeneity at submicron resolution. It is worth noting that routine laboratory techniques, such as HIAC and MFI, often require sample dilution to enhance the refractive index contrast when measuring high-concentration biological formulations.[44] As a spectroscopic imaging technique, SRS can potentially analyze samples as-is at a high protein concentration.

Although SRS microscopy does not require extrinsic labeling and sample modification, imaging drug solution by scanning the microscope field of view has a very low throughput. To combat this limitation, we opted to filter the drug solution to both immobilize and enrich particle counts. By directly imaging the immobilized particles on the filter, we found that silicone oil−protein particles have varying morphology. Some mixture particles appear as clumps, whereas others appear as strands coming off a silicone oil droplet. The demonstrated chemical information from SRS microscopy is an additional dimension of information to study these particles that is complementary to traditional morphological methods.

The SRS imaging filtration method is not without limitations. The two filters demonstrated both showed unique problems. The Anodisk filter had large amounts of contaminating particles that complicated analysis and the PC filter had a Raman spectrum that overlapped with the protein Raman signature at 2930 cm^{-1}. For future improvement upon this imaging method, additional filters can be tested to mitigate contamination or spectral overlap problems. The filtration imaging process vastly increases the imaging throughput of particles, but potential problems can occur with this process. First, it is not known whether filtration can alter or generate particles. Potentially, silicone oil can coat proteinaceous particles as it flows through the filter. Second, it is difficult to validate the accuracy of the spectral fittings because of the lack of control over how much mixing can occur in a particle. Additionally, even though the filter membranes used had a pore size of 0.2 μm, we had some difficulty imaging very small particles ~1 μm in size as these particles commonly floated in and out of focus. Finally, it is important to note that this was a case study of etanercept, meaning different results may occur when this SRS technique is applied to other biopharmaceutical drugs. Nevertheless, the method developed has the potential to provide insights into the mechanism of protein aggregation and screen drug formulations.

Through the SRS imaging method, we are able to visualize intraparticle compositional heterogeneity with high spatial resolution. Silicone oil−protein mixtures have significantly different intraparticle morphologies, strongly indicating that particle classifications that rely solely on morphological features are likely to be inaccurate for particle mixtures. Additionally, through a spectral fitting at a pixel level, we found that over 90% of imaged particles have >10% composition of silicone oil. These findings suggest that silicone oil and drug active ingredient proteins can interact to form silicone oil−protein mixtures. The ability to observe this interaction at high resolution is critical to understand the dynamics of aggregation. Future studies will focus on understanding the particle formation dynamics by comparing samples prepared under different stress conditions. As SRS is nonperturbative, it is also possible to continuously image particles in solution to test conditions such as temperature and pH over time on drug product stability. Coatings could be applied to the microscope cover glass or cover slip to immobilize particles for high throughput imaging in the solution. Alternatively, an SRS-based MFI method can be adapted to both have high throughput imaging and spectral information without altering the particle environment.[45] Such a flow-based method would also directly address many of the issues associated with imaging on a filter membrane.

ASSOCIATED CONTENT

Supporting Information

The Supporting Information is available free of charge at https://pubs.acs.org/doi/10.1021/acs.molpharmaceut.3c00391.

Stimulated Raman scattering (SRS) imaging and accompanying spectra of silicone oil basis component; SRS spectra of contaminating particles in Anodisk filtration; SRS image of chemically heterogeneous silicone oil−protein mixture particle with SRS spectra taken from two separate areas; and additional SRS images of particles on polycarbonate (PC) filter with spectra (PDF)

AUTHOR INFORMATION

Corresponding Authors

Xi Zhao − *Analytical Enabling Capabilities, Analytical Research and Development and Sterile and Specialty*

https://doi.org/10.1021/acs.molpharmaceut.3c00391
Mol. Pharmaceutics 2023, 20, 4268−4276

Products, Pharmaceutical Sciences & Clinical Supply, Merck & Co., Inc., Rahway, New Jersey 07065, United States; Email: xi.zhao1@merck.com

Dan Fu − *Department of Chemistry, University of Washington, Seattle, Washington 98195, United States*; orcid.org/0000-0001-9243-8306; Email: danfu@uw.edu

Authors

Brian Wong − *Department of Chemistry, University of Washington, Seattle, Washington 98195, United States*

Yongchao Su − *Analytical Enabling Capabilities, Analytical Research and Development, Merck & Co., Inc., Rahway, New Jersey 07065, United States*; orcid.org/0000-0001-5063-3218

Hanlin Ouyang − *Analytical Enabling Capabilities, Analytical Research and Development, Merck & Co., Inc., Rahway, New Jersey 07065, United States*

Timothy Rhodes − *Analytical Enabling Capabilities, Analytical Research and Development, Merck & Co., Inc., Rahway, New Jersey 07065, United States*

Wei Xu − *Analytical Enabling Capabilities, Analytical Research and Development, Merck & Co., Inc., Rahway, New Jersey 07065, United States*

Hanmi Xi − *Analytical Enabling Capabilities, Analytical Research and Development, Merck & Co., Inc., Rahway, New Jersey 07065, United States*

Complete contact information is available at: https://pubs.acs.org/10.1021/acs.molpharmaceut.3c00391

Author Contributions

The manuscript was written through the contributions of all authors. All authors have given approval to the final version of the manuscript.

Notes

The authors declare no competing financial interest.

■ ACKNOWLEDGMENTS

We thank Shuaiqian Men for performing the initial test of SRS imaging of protein formulations. This work was funded by the NSF CAREER 1846503 and the Eli Lilly Young Investigator Award to D.F., and by a research grant from Merck Sharp & Dohme LLC, a subsidiary of Merck & Co., Inc., Rahway, NJ, USA to D.F.

■ REFERENCES

(1) Leader, B.; Baca, Q. J.; Golan, D. E. Protein Therapeutics: A Summary and Pharmacological Classification. *Nat. Rev. Drug Discov.* **2008**, *7*, 21−39.

(2) Chisholm, C. F.; Soucie, K. R.; Song, J. S.; Strauch, P.; Torres, R. M.; Carpenter, J. F.; Ragheb, J. A.; Randolph, T. W. Immunogenicity of Structurally Perturbed Hen Egg Lysozyme Adsorbed to Silicone Oil Microdroplets in Wild-Type and Transgenic Mouse Models. *J. Pharm. Sci.* **2017**, *106*, 1519−1527.

(3) Moussa, E. M.; Panchal, J. P.; Moorthy, B. S.; Blum, J. S.; Joubert, M. K.; Narhi, L. O.; Topp, E. M. Immunogenicity of Therapeutic Protein Aggregates. *J. Pharm. Sci.* **2016**, *105*, 417−430.

(4) Lundahl, M. L. E.; Fogli, S.; Colavita, P. E.; Scanlan, E. M. Aggregation of Protein Therapeutics Enhances Their Immunogenicity: Causes and Mitigation Strategies. *RSC Chem. Biol.* **2021**, *2*, 1004−1020.

(5) Bhatnagar, B. S.; Bogner, R. H.; Pikal, M. J. Protein Stability During Freezing: Separation of Stresses and Mechanisms of Protein Stabilization. *Pharm. Dev. Technol.* **2007**, *12*, 505−523.

(6) Chi, E. Y.; Krishnan, S.; Randolph, T. W.; Carpenter, J. F. Physical Stability of Proteins in Aqueous Solution: Mechanism and Driving Forces in Nonnative Protein Aggregation. *Pharm. Res.* **2003**, *20*, 1325−1336.

(7) Mahler, H.-C.; Friess, W.; Grauschopf, U.; Kiese, S. Protein Aggregation: Pathways, Induction Factors and Analysis. *J. Pharm. Sci.* **2009**, *98*, 2909−2934.

(8) Center for Drug Evaluation and Research. *Inspection of Injectable Products for Visible Particulates*; U.S. Food and Drug Administration. https://www.fda.gov/regulatory-information/search-fda-guidance-documents/inspection-injectable-products-visible-particulates (accessed 2022-12-06).

(9) McKoy, J. M.; Stonecash, R. E.; Cournoyer, D.; Rossert, J.; Nissenson, A. R.; Raisch, D. W.; Casadevall, N.; Bennett, C. L. Epoetin-Associated Pure Red Cell Aplasia: Past, Present, and Future Considerations. *Transfusion* **2008**, *48*, 1754−1762.

(10) Chisholm, C. F.; Baker, A. E.; Soucie, K. R.; Torres, R. M.; Carpenter, J. F.; Randolph, T. W. Silicone Oil Microdroplets Can Induce Antibody Responses Against Recombinant Murine Growth Hormone in Mice. *J. Pharm. Sci.* **2016**, *105*, 1623−1632.

(11) Roberts, C. J. Therapeutic Protein Aggregation: Mechanisms, Design, and Control. *Trends Biotechnol.* **2014**, *32*, 372−380.

(12) Panchal, J.; Kotarek, J.; Marszal, E.; Topp, E. M. Analyzing Subvisible Particles in Protein Drug Products: A Comparison of Dynamic Light Scattering (DLS) and Resonant Mass Measurement (RMM). *AAPS J.* **2014**, *16*, 440−451.

(13) Tatford, O. C.; Gomme, P. T.; Bertolini, J. Analytical Techniques for the Evaluation of Liquid Protein Therapeutics. *Biotechnol. Appl. Biochem.* **2004**, *40*, 67−81.

(14) den Engelsman, J.; Garidel, P.; Smulders, R.; Koll, H.; Smith, B.; Bassarab, S.; Seidl, A.; Hainzl, O.; Jiskoot, W. Strategies for the Assessment of Protein Aggregates in Pharmaceutical Biotech Product Development. *Pharm. Res.* **2011**, *28*, 920−933.

(15) Gerhardt, A.; Nguyen, B. H.; Lewus, R.; Carpenter, J. F.; Randolph, T. W. Effect of the Siliconization Method on Particle Generation in a Monoclonal Antibody Formulation in Pre-Filled Syringes. *J. Pharm. Sci.* **2015**, *104*, 1601−1609.

(16) Wang, T.; Richard, C. A.; Dong, X.; Shi, G. H. Impact of Surfactants on the Functionality of Prefilled Syringes. *J. Pharm. Sci.* **2020**, *109*, 3413−3422.

(17) Shi, G. H.; Gopalrathnam, G.; Shinkle, S. L.; Dong, X.; Hofer, J. D.; Jensen, E. C.; Rajagopalan, N. Impact of Drug Formulation Variables on Silicone Oil Structure and Functionality of Prefilled Syringe System. *PDA J. Pharm. Sci. Technol.* **2018**, *72*, 50−61.

(18) Kiyoshi, M.; Tada, M.; Shibata, H.; Aoyama, M.; Ishii-Watabe, A. Characterization of Aggregated Antibody-Silicone Oil Complexes: From Perspectives of Morphology, 3D Image, and Fcγ Receptor Activation. *J. Pharm. Sci.* **2021**, *110*, 1189−1196.

(19) Probst, C. Characterization of Protein Aggregates, Silicone Oil Droplets, and Protein-Silicone Interactions Using Imaging Flow Cytometry. *J. Pharm. Sci.* **2020**, *109*, 364−374.

(20) Maruno, T.; Watanabe, H.; Yoneda, S.; Uchihashi, T.; Adachi, S.; Arai, K.; Sawaguchi, T.; Uchiyama, S. Sweeping of Adsorbed Therapeutic Protein on Prefillable Syringes Promotes Micron Aggregate Generation. *J. Pharm. Sci.* **2018**, *107*, 1521−1529.

(21) Torisu, T.; Maruno, T.; Yoneda, S.; Hamaji, Y.; Honda, S.; Ohkubo, T.; Uchiyama, S. Friability Testing as a New Stress-Stability Assay for Biopharmaceuticals. *J. Pharm. Sci.* **2017**, *106*, 2966−2978.

(22) Barnard, J. G.; Babcock, K.; Carpenter, J. F. Characterization and Quantitation of Aggregates and Particles in Interferon-β Products: Potential Links Between Product Quality Attributes and Immunogenicity. *J. Pharm. Sci.* **2013**, *102*, 915−928.

(23) Yoneda, S.; Torisu, T.; Uchiyama, S. Development of Syringes and Vials for Delivery of Biologics: Current Challenges and Innovative Solutions. *Expert Opin. Drug Deliv.* **2021**, *18*, 459−470.

(24) Krayukhina, E.; Tsumoto, K.; Uchiyama, S.; Fukui, K. Effects of Syringe Material and Silicone Oil Lubrication on the Stability of Pharmaceutical Proteins. *J. Pharm. Sci.* **2015**, *104*, 527−535.

(25) Strehl, R.; Rombach-Riegraf, V.; Diez, M.; Egodage, K.; Bluemel, M.; Jeschke, M.; Koulov, A. V. Discrimination Between Silicone Oil Droplets and Protein Aggregates in Biopharmaceuticals: A Novel Multiparametric Image Filter for Sub-Visible Particles in Microflow Imaging Analysis. *Pharm. Res.* **2012**, *29*, 594−602.
(26) Probst, C.; Zayats, A.; Venkatachalam, V.; Davidson, B. Advanced Characterization of Silicone Oil Droplets in Protein Therapeutics Using Artificial Intelligence Analysis of Imaging Flow Cytometry Data. *J. Pharm. Sci.* **2020**, *109*, 2996−3005.
(27) Huang, C.-T.; Sharma, D.; Oma, P.; Krishnamurthy, R. Quantitation of Protein Particles in Parenteral Solutions Using Micro-Flow Imaging. *J. Pharm. Sci.* **2009**, *98*, 3058−3071.
(28) Weinbuch, D.; Jiskoot, W.; Hawe, A. Light Obscuration Measurements of Highly Viscous Solutions: Sample Pressurization Overcomes Underestimation of Subvisible Particle Counts. *AAPS J.* **2014**, *16*, 1128−1131.
(29) Sharma, D. K.; King, D.; Oma, P.; Merchant, C. Micro-Flow Imaging: Flow Microscopy Applied to Sub-Visible Particulate Analysis in Protein Formulations. *AAPS J.* **2010**, *12*, 455−464.
(30) Weinbuch, D.; Zölls, S.; Wiggenhorn, M.; Friess, W.; Winter, G.; Jiskoot, W.; Hawe, A. Micro−Flow Imaging and Resonant Mass Measurement (Archimedes) − Complementary Methods to Quantitatively Differentiate Protein Particles and Silicone Oil Droplets. *J. Pharm. Sci.* **2013**, *102*, 2152−2165.
(31) Cheng, J.-X.; Xie, X. S. Vibrational Spectroscopic Imaging of Living Systems: An Emerging Platform for Biology and Medicine. *Science* **2015**, *350*, aaa8870.
(32) Fu, D. Quantitative Chemical Imaging with Stimulated Raman Scattering Microscopy. *Curr. Opin. Chem. Biol.* **2017**, *39*, 24−31.
(33) Fu, D.; Zhou, J.; Zhu, W. S.; Manley, P. W.; Wang, Y. K.; Hood, T.; Wylie, A.; Xie, X. S. Imaging the Intracellular Distribution of Tyrosine Kinase Inhibitors in Living Cells with Quantitative Hyperspectral Stimulated Raman Scattering. *Nat. Chem.* **2014**, *6*, 614−622.
(34) Zhang, D.; Wang, P.; Slipchenko, M. N.; Ben-Amotz, D.; Weiner, A. M.; Cheng, J.-X. Quantitative Vibrational Imaging by Hyperspectral Stimulated Raman Scattering Microscopy and Multivariate Curve Resolution Analysis. *Anal. Chem.* **2013**, *85*, 98−106.
(35) Slipchenko, M. N.; Chen, H.; Ely, D.; Jung, Y.; Carvajal, M. T.; Cheng, J.-X. Vibrational Imaging of Tablets by Epi-Detected Stimulated Raman Scattering Microscopy. *Analyst* **2010**, *135*, 2613−2619.
(36) Francis, A. T.; Nguyen, T. T.; Lamm, M. S.; Teller, R.; Forster, S. P.; Xu, W.; Rhodes, T.; Smith, R. L.; Kuiper, J.; Su, Y.; Fu, D. In Situ Stimulated Raman Scattering (SRS) Microscopy Study of the Dissolution of Sustained-Release Implant Formulation. *Mol. Pharmaceutics* **2018**, *15*, 5793.
(37) Figueroa, B.; Nguyen, T.; Sotthivirat, S.; Xu, W.; Rhodes, T.; Lamm, M. S.; Smith, R. L.; John, C. T.; Su, Y.; Fu, D. Detecting and Quantifying Microscale Chemical Reactions in Pharmaceutical Tablets by Stimulated Raman Scattering Microscopy. *Anal. Chem.* **2019**, *91*, 6894−6901.
(38) Fu, D.; Holtom, G.; Freudiger, C.; Zhang, X.; Xie, X. S. Hyperspectral Imaging with Stimulated Raman Scattering by Chirped Femtosecond Lasers. *J. Phys. Chem. B* **2013**, *117*, 4634−4640.
(39) Xu, F. X.; Rathbone, E. G.; Fu, D. Simultaneous Dual-Band Hyperspectral Stimulated Raman Scattering Microscopy with Femtosecond Optical Parametric Oscillators. *J. Phys. Chem. B* **2023**, *127*, 2187−2197.
(40) Fu, D.; Xie, X. S. Reliable Cell Segmentation Based on Spectral Phasor Analysis of Hyperspectral Stimulated Raman Scattering Imaging Data. *Anal. Chem.* **2014**, *86*, 4115−4119.
(41) Oßmann, B. E.; Sarau, G.; Schmitt, S. W.; Holtmannspötter, H.; Christiansen, S. H.; Dicke, W. Development of an Optimal Filter Substrate for the Identification of Small Microplastic Particles in Food by Micro-Raman Spectroscopy. *Anal. Bioanal. Chem.* **2017**, *409*, 4099−4109.
(42) Zada, L.; Leslie, H. A.; Vethaak, A. D.; Tinnevelt, G. H.; Jansen, J. J.; de Boer, J. F.; Ariese, F. Fast Microplastics Identification with Stimulated Raman Scattering Microscopy. *J. Raman Spectrosc.* **2018**, *49*, 1136−1144.
(43) Krayukhina, E.; Yokoyama, M.; Hayashihara, K. K.; Maruno, T.; Noda, M.; Watanabe, H.; Uchihashi, T.; Uchiyama, S. An Assessment of the Ability of Submicron- and Micron-Size Silicone Oil Droplets in Dropped Prefillable Syringes to Invoke Early- and Late-Stage Immune Responses. *J. Pharm. Sci.* **2019**, *108*, 2278−2287.
(44) Demeule, B.; Messick, S.; Shire, S. J.; Liu, J. Characterization of Particles in Protein Solutions: Reaching the Limits of Current Technologies. *AAPS J.* **2010**, *12*, 708−715.
(45) Hiramatsu, K.; Ideguchi, T.; Yonamine, Y.; Lee, S.; Luo, Y.; Hashimoto, K.; Ito, T.; Hase, M.; Park, J.-W.; Kasai, Y.; Sakuma, S.; Hayakawa, T.; Arai, F.; Hoshino, Y.; Goda, K. High-Throughput Label-Free Molecular Fingerprinting Flow Cytometry. *Sci. Adv.* **2019**, *5*, No. eaau0241.

https://doi.org/10.1021/acs.molpharmaceut.3c00391
Mol. Pharmaceutics 2023, 20, 4268−4276